

# Microstructure and properties of Cu-Sn-Zn-TiO<sub>2</sub> Nano-composite coatings on mild steel

Weidong Gao<sup>1</sup>, Di Cao<sup>1</sup>, Yunxue Jin<sup>1</sup>, Xiaowei Zhou<sup>1</sup>, Guang Cheng<sup>2\*</sup>, Yuxin Wang<sup>1\*</sup>

<sup>1</sup> School of Materials Science and Engineering, Jiangsu University of Science and Technology, Zhenjiang, 212003, Jiangsu, China

<sup>2</sup> Physical and Computational Sciences Directorate, Pacific Northwest National Laboratory, P.O. Box 999, Richland, WA, 99352, USA

**Abstract:** Cu-Sn-Zn coatings have been widely used in industry for their unique properties, such as good conductivity, high corrosion resistance and excellent solderability. To further improve the mechanical performance of Cu-Sn-Zn coatings, powder-enhanced method was applied in the current study and Cu-Sn-Zn-TiO<sub>2</sub> nano-composite coatings with different TiO<sub>2</sub> concentration were fabricated. The microstructure of Cu-Sn-Zn-TiO<sub>2</sub> nano-composite coatings were investigated by X-ray diffraction (XRD) and Scanning Electron Microscopy (SEM). The mechanical properties of coatings including microhardness and wear resistance were studied. The results indicate that the incorporation of TiO<sub>2</sub> nanoparticle can significantly influence the properties of Cu-Sn-Zn coatings. The microhardness of Cu-Sn-Zn coating was increased to 383 HV from 330 HV with 1g/L TiO<sub>2</sub> addition. Also, the corrosion resistance of coating was enhanced. The effects of TiO<sub>2</sub> nanoparticle concentration on the microstructure, mechanical properties and corrosion resistance of Cu-Sn-Zn-TiO<sub>2</sub> nano-composite coatings were discussed.

**Keywords:** Cu-Sn-Zn ternary alloy; Nano-composite coatings; Mechanical property; Corrosion resistance

---

\* Corresponding authors.

Email address: [ywan943@163.com](mailto:ywan943@163.com) (Yuxin Wang) [septem88@hotmail.com](mailto:septem88@hotmail.com) (Guang Cheng).

## 1. Introduction

Copper-tin-zinc (Cu-Sn-Zn) ternary alloy has attracted tremendous research interests due to its unique properties, including gorgeous color, high corrosion resistance [1, 2], remarkable solder ability [3-6] and good electrical conductivity. Cu-Sn-Zn alloys have been fabricated by different methods, such as melting [7-11], powder metallurgy [12] and electrodeposition [13-16]. Among these methods, electrodeposition is an effective method to fabricate Cu-Sn-Zn coatings [17, 18] because of its simple process and high environment adaptability. In addition, the properties and color of coatings can be easily controlled by adjusting the plating parameters. The plating bath of Cu-Sn-Zn coatings mainly includes alkaline cyanide solution and acid sulphate solution. The cyanide solution is the most common bath used in the electronic applications, while the environmentally-friendly acid sulphate bath is widely adopted for decorative purpose.

Comparing with the Chromium (Cr) [19] or Nickel (Ni) [20, 21], which are the mostly used coating, Cu-Sn-Zn coating possesses a relatively soft hardness. In order to improve the mechanical properties and explore the application of Cu-Sn-Zn coatings, the preparation of Cu-Sn-Zn based nano-composite coatings, i.e., incorporating the second phase or other nanoparticles into coating matrix, could be a potential solution [20-23]. It is well known that if nano-sized particles such as oxides, carbides and polytetrafluoroethylene highly disperse into Cu-Sn-Zn coating matrix, the properties especially mechanical strength will be improved dramatically. The corresponding strengthening mechanism can be attributed to the grain refinement and dispersion strengthening.

An ideal Cu-Sn-Zn coating prepared for decoration field should have a long service life so both wear resistance and corrosion resistance should meet certain design requirements. Among various reinforcement choices,  $\text{TiO}_2$  was selected due to its encouraging effect on microstructural, hardness, wear resistance and corrosion resistance of Ni-P coatings [21]. Furthermore, the preparation of  $\text{TiO}_2$  added Cu-Sn-Zn coatings via environmentally-friendly acid sulphate bath have not been studied. In the

present research, a systematic study of Cu-Sn-Zn-TiO<sub>2</sub> nano-composite coatings (with a TiO<sub>2</sub> concentration of 0-5 g/L) has been conducted. The influences of TiO<sub>2</sub> nanoparticles concentration on the microstructure, mechanical properties and corrosion resistance were discussed.

## **2. Experimental details**

### **2.1 Sample Preparation**

All the coatings were electroplated onto the hot-dipping galvanized mild steel substrates (0.2×20×30mm<sup>3</sup>). The substrates were first dipped into a HCL solution (>10%) for 5 mins at room temperature to remove the covered Zn layer. The specimens were electroplated after rinse thoroughly by distilled water.

The electroplating system contains a mild steel sample as the cathode and a Cu plate as the anode. The bath composition and plating parameters are given in Table 1. The basic Cu-Sn-Zn plating bath was prepared using Sigma analytical grade reagents. The PH value of bath was adjusted to 8.6 (±0.2) by H<sub>2</sub>SO<sub>4</sub> or KOH. TiO<sub>2</sub> powder with an average diameter of 10 nm was added into the electrolyte bath. The bath solution was continuously stirred at a rate of 300 rpm for 20 min by magnetic stirring in order to achieve a good suspension. Six different concentrations of TiO<sub>2</sub> powders between 0 and 5 g/ L were selected in order to achieve the best properties. For easy description, Cu-Sn-Zn-x TiO<sub>2</sub> is adopted to represent the coatings containing different TiO<sub>2</sub>. Pure Cu-Sn-Zn coatings were also prepared by direct deposition under the same conditions for comparison purpose.

### **2.2 Sample Characterization**

The phase structure and preferred orientation of coatings were determined by X-ray diffraction (XRD) patterns using Bruker D2 Phaser diffractometer (V = 30 kV, I = 15 mA) with the Cu K $\alpha$  radiation ( $\lambda$  = 0.15406 nm). Diffraction patterns were recorded in the 2 $\theta$  range from 20° to 90° at a scanning rate of 1° min<sup>-1</sup>. The morphology of as-

deposited surface and composition of coatings were analyzed using a Zeiss field emission scanning electron microscope (Gemini SEM 300, Zeiss, Germany). The samples were cold mounted using Epoxy resin (ration of resin: hardener, 3:1) to obtain the cross-section images. The backscattered electrons were analyzed with a solid state detector to examine the interface between the substrate and coatings.

Vickers microhardness tests were conducted using a load of 50 g with a holding time of 15 s. The hardness values were calculated based on 10 measurements. Each indents were carried out on the surface with sufficient space between indents to eliminate the residual stress. The indent will cover a large region, i.e., over  $20 \mu\text{m}^2$  so the average properties within a large region will be obtained from microhardness test and the indentation surface roughness could be ignored because of the indentation depth [24-27]. The tribological properties of the coatings were tested using a micro-tribometer (UMT-2, CETR, USA) in air at room temperature, relative humidity of ~50% and under dry, non-lubricated conditions. The samples were tested linearly and a steel ball with a diameter of 9.58 mm was used as the counter surface. The load and total sliding distance of each wear test were set to 3N and 3m, respectively. The sliding wear test was conducted three times for each sample. The wear track images of coatings were observed by a high-resolution optical microscope.

The corrosion resistance of coatings were measured by an electrochemical workstation (CS2350, CorrTest, China). All corrosion tests were performed at room temperature (25°C) using a three-electrode system with platinum mesh as auxiliary electrode, Ag/AgCl/KCl (sat.) electrode (0.197 Vs the Standard Hydrogen Electrode-SHE) with Luggin probe as the reference electrode and coated specimen as working electrode. The exposed surface area of all samples was set to  $1 \text{ cm}^2$ . The potentiodynamic polarization tests were conducted at a constant scanning speed of  $1 \text{ mV s}^{-1}$ . The corrosion current density and corrosion potential were determined based on Tafel's extrapolation. All the corrosion tests were performed at ambient temperature in 3.5 wt.% NaCl solution.

### 3. Results and discussion

#### 3.1 Phase Structure of Coatings

The X-ray diffraction patterns of Cu-Sn-Zn-x TiO<sub>2</sub> (x=0, 1, 2, 3, 4 and 5 g/L) nano-composite coatings are shown in Fig. 1. It can be observed that all the XRD patterns imply four prominent peaks which corresponding to the Cu<sub>0.6</sub>Sn<sub>0.1</sub>Zn<sub>0.3</sub> according to the phase identification. The peaks at 25.4° can be assigned to (101) plane of anatase, indicating that the TiO<sub>2</sub> nanoparticle was incorporated into the coatings. There was no TiO<sub>2</sub> peaks can be detected in Cu-Sn-Zn-1g/L TiO<sub>2</sub> and Cu-Sn-Zn-2g/L TiO<sub>2</sub> coatings due to the low quantity of TiO<sub>2</sub> particles and high intensity of other diffraction peaks.

#### 3.2 Surface Morphology and Cross-Section of Coatings

Fig. 2 presents the surface morphologies of Cu-Sn-Zn-TiO<sub>2</sub> nano-composite coatings with different powder addition. The surface of pure Cu-Sn-Zn coating is relatively plain and homogeneous, as shown in Fig. 2(a). No remarkable variation can be observed on the surface of Cu-Sn-Zn-1g/L TiO<sub>2</sub> coating except some small nodules, as shown in Fig. 2(b). Further increasing TiO<sub>2</sub> concentration leads to the increase of black spots and blurry areas on the coating surface. Observation of higher magnification image confirm that the black spots depict particle agglomeration and the blurry areas represent voids in the coating. As the size of TiO<sub>2</sub> nanoparticles used for this research is very tiny (~10nm), serious TiO<sub>2</sub> particle agglomeration occurred in the Cu-Sn-Zn coating matrix, as shown in Fig. 2(b)-(f).

Fig. 3 depicts the cross-section microstructure of Cu-Sn-Zn and Cu-Sn-Zn-1g/L TiO<sub>2</sub> nano-composite coatings. A gleaming boundary between the coating and the steel substrate can be observed. No abrasion or cracks exist at the interfaces of the coatings, indicating a good adhesion between the steel substrate and coating. All coatings present a similar thickness of approximately 15 μm. The deposition rate of coatings remains constant after adding TiO<sub>2</sub> nanoparticle. No obvious TiO<sub>2</sub> nanoparticles were seen in the cross-section which probably due to their small size and relatively low content. This

phenomenon is consistent with the XRD analysis as shown in Fig. 1 and Fig. 2(b).

### 3.3 Microhardness and Wear Resistance of Coatings

Fig. 4 shows the correlation between the microhardness of Cu-Sn-Zn-TiO<sub>2</sub> nano-composite coatings and TiO<sub>2</sub> concentration in the bath. Initially, the microhardness of pure Cu-Sn-Zn coating was ~330 HV<sub>50</sub>, much higher than the hardness of mild steel substrate, ~110 HV<sub>50</sub>. Also, the small hardness deviation indicates a homogenized microstructure was prepared in the current method. With the 1g/L addition of TiO<sub>2</sub> nanoparticles to the bath, the hardness of Cu-Sn-Zn-1g/L TiO<sub>2</sub> coating reaches to the peak value, ~382 HV<sub>50</sub>. Compared to the initial Cu-Sn-Zn coating, the hardness increased ~16%. The improvement of microhardness was attributed to the highly dispersed TiO<sub>2</sub> nanoparticles in the Cu-Sn-Zn matrix as shown in Fig. 2b and 3b. The introduced nanoparticles will increase the local dislocation density and refine the grain size. Also, the pinning effect of these nanoparticles will block the movement of the dislocations so as to raise the yield strength or the hardness of the coatings [28, 29]. However, higher TiO<sub>2</sub> concentration in the bath did not raise the hardness of the coatings. The microhardness of the coating was reduced to ~333 HV<sub>50</sub>, ~325 HV<sub>50</sub>, and ~320 HV<sub>50</sub> with 2g/L TiO<sub>2</sub>, 3g/L TiO<sub>2</sub>, and 4g/L TiO<sub>2</sub>, respectively. The microhardness was reduced to ~300 HV<sub>50</sub> for Cu-Sn-Zn-5g/L TiO<sub>2</sub> coatings. Too many particles will easily lead to agglomeration and voids between particles were generated in the deposition processing as the highlighted spots shown in Fig. 2 (c), (d), (e), and (f). Those voids could significantly reduce the hardness. Hence, the competition between particles dispersion hardening and possible voids among particles determine the final hardness of the nano-composite coatings.

The wear resistance abilities of the three nano-composite coatings were tested and compared. In the dry sliding wear test, a higher hardness value brought a smaller contact area between coatings and the steel ball. So different wear tracks, 391 μm, 265 μm, and 516 μm, were observed in Cu-Sn-Zn, Cu-Sn-Zn-1g/L TiO<sub>2</sub>, and Cu-Sn-Zn-5g/L TiO<sub>2</sub>, respectively, as illustrated in Fig.5. The correlation between the width of wear track

and hardness is quite clear. Meanwhile, different surface morphologies after wear test are observed for the three coatings because of different microstructures. Significant plowing lines and several wear debris on the worn surface were observed in Fig.5 (a). The matrix of the current Cu-Sn-Zn coating is dominant by  $\text{Cu}_{0.6}\text{Sn}_{0.1}\text{Zn}_{0.3}$ , which would be quite stiff. So the main wear mechanism of Cu-Sn-Zn coating is adhesive wear, which is quite common among electroplated metallic coatings [30-32]. After adding 1g/L  $\text{TiO}_2$  sol into the plating solution, the contact area in the wear test reduced a lot and the plough-lines became much shallower and more uniform than the Cu-Sn-Zn coating. In addition, the wear debris was not observed in Fig.5 (b). The different surface morphologies demonstrated the reinforcement effect of nanoparticle: the embedded  $\text{TiO}_2$  nanoparticles would polish the frictional surface, and homogenize the contact stress distribution between the frictional counter bodies during the wear process. With more  $\text{TiO}_2$  sol into the plating solution, the voids among particle clusters raised the contact area very much. Thicker and deeper plowing lines were observed in Fig.5 (c) compared to other two samples. Also, plenty of wear debris were observed on the sliding surface.

Then, the wear volume loss of three coatings was summarized in Fig. 6. As expectation, the wear volume loss fraction for Cu-Sn-Zn-1g/L  $\text{TiO}_2$  is  $\sim 0.7 \times 10^{-13} \text{ m}^3$ , which is the smallest among tested samples. The volume loss of Cu-Sn-Zn and Cu-Sn-Zn-5g/L  $\text{TiO}_2$  are  $\sim 2.4 \times 10^{-13} \text{ m}^3$  and  $\sim 7.2 \times 10^{-13} \text{ m}^3$ , respectively. According to the Archard's law, the volume loss during sliding wear is inversely proportional to the material hardness and proportional to the friction coefficient [33-36]. Because of the similar surface roughness in the current study, the friction coefficient of different coatings are quite similar. Thus, the volume loss among different coatings would directly reflect the differences between hardness. It should be noted that the Vickers hardness test would penetrate the coating-substrate system for over 5  $\mu\text{m}$  under 50 g load which has already exceeded the 10% thickness of the coating [23, 37, 38]. On this condition, the soft mild steel substrate has affected the hardness values. The actual hardness difference between

Cu-Sn-Zn-1g/L TiO<sub>2</sub> and Cu-Sn-Zn should be much more than 16% if the substrate effect was removed. Hence, indentation study with penetration depth less than 1 μm will be conducted in the future.

### 3.4 Corrosion Resistance of Coatings

Fig. 7 presents the polarization curves of Cu-Sn-Zn, Cu-Sn-Zn-1g/L TiO<sub>2</sub> and Cu-Sn-Zn-5g/L TiO<sub>2</sub> nano-composite coatings. The corresponding electrochemical properties, including corrosion potentials, corrosion current densities and corrosion rates of coatings were calculated by fitting potentiodynamic curves as listed in Table 2.

The corrosion potentials ( $E_{corr}$ ) of three coatings were approximately the same, around -0.256 V. The corrosion current densities ( $I_{corr}$ ) and corrosion rates of coatings varied with the concentration of TiO<sub>2</sub> addition. The  $I_{corr}$  and corrosion rate of Cu-Sn-Zn coating were ~ 8.353 μA/cm<sup>2</sup> and 0.098 mm/a, while the  $I_{corr}$  and corrosion rate value obtained for Cu-Sn-Zn-1g/L TiO<sub>2</sub> coating were ~ 6.284 μA/cm<sup>2</sup> and 0.074 mm/a, respectively, indicating an improved corrosion resistance. The improvement of corrosion resistance could be attributed to the dense structure of coating and the uniform distribution of TiO<sub>2</sub> nanoparticles in coating matrix. However, more TiO<sub>2</sub> nanopowder addition will cause a deterioration of corrosion resistance for the coatings due to the serious particle agglomeration and porous microstructure. Cu-Sn-Zn-5g/L TiO<sub>2</sub> coating exhibits highest  $I_{corr}$  and the fastest corrosion rate, ~ 9.191 μA/cm<sup>2</sup> and 0.108 mm/a, respectively. The results of Tafel plots show a same tendency with the mechanical properties of coatings.

## 4. Conclusions

Cu-Sn-Zn-TiO<sub>2</sub> nano-composite coatings were produced by electrodeposition method using acid sulfate bath. Their microstructure, mechanical properties and corrosion resistance were systematically investigated. Proper inclusion of TiO<sub>2</sub> nanoparticles into Cu-Sn-Zn matrix provides a decent strengthening effect and significantly improves the properties of coatings. Compared to the pure Cu-Sn-Zn coating, the microhardness of

Cu-Sn-Zn-1g/L TiO<sub>2</sub> coating was increased by ~16%. Meanwhile, the corresponding wear resistance and corrosion resistance have also been greatly enhanced. Future study will focus on developing new Cu-Sn-Zn based nano-composite coatings by reducing the agglomeration of particles in the deposition process to prepare densified coatings. Meanwhile, the composition optimization and more characterizations methods, i.e., high-resolution transmission electron microscopy (HRTEM) [22, 23], resonance ultrasound spectroscopy [39-41], etc., will be attempted to better understand its microstructure.

### **Acknowledgments**

This research was supported by National Natural Science Foundation of China (51601073), Jiangsu Distinguished Professor Project (1064901601) and Start research fund of Jiangsu University of Science and Technology (1624821607-5). Pacific Northwest National Laboratory (PNNL) is operated by Battelle Memorial Institute for the US Department of Energy (DOE) under Contract No. DE-AC06-76RL01830. The authors would like to express our gratitude to Mr. Haixin Zhu, Mr. Lin Zhang and technical staff in Jinshi Electroplating Ltd.

## Tables

Table 1 Bath composition and processing parameters of electrodeposited Cu-Sn-Zn-TiO<sub>2</sub> and Cu-Sn-Zn coatings.

Bath composition & plating parameters	Quantity
CuSO <sub>4</sub>	35g/L
SnCl <sub>2</sub>	3 g/L
ZnSO <sub>4</sub>	10g/L
K <sub>4</sub> P <sub>2</sub> O <sub>7</sub>	260 g/L
NaH <sub>2</sub> PO <sub>4</sub> ·2H <sub>2</sub> O	10g/L
C <sub>6</sub> H <sub>5</sub> K <sub>3</sub> O <sub>7</sub>	25g/L
KNaC <sub>4</sub> H <sub>4</sub> O <sub>6</sub> ·4H <sub>2</sub> O	25 g/L
Saccharin	0.04 g/L
Temperature	32 °C
Current density	20 mA/cm <sup>2</sup>
Agitation speed	300 rpm
Plating time	60 min
TiO <sub>2</sub> nanoparticles	0, 1g/L, 2g/L, 3 g/L, 4 g/L, 5 g/L

Table 2 Corrosion parameters derived from analysis of potentiodynamic linear polarization curves

Sample	E <sub>corr</sub> (V)	I <sub>corr</sub> ( $\mu\text{Acm}^{-2}$ )	Corrosion Rate (mm/a)
Cu-Sn-Zn	-0.253	8.353	0.098
Cu-Sn-Zn-1g/L TiO <sub>2</sub>	-0.256	6.284	0.074
Cu-Sn-Zn-5g/L TiO <sub>2</sub>	-0.259	9.191	0.108

## Figures

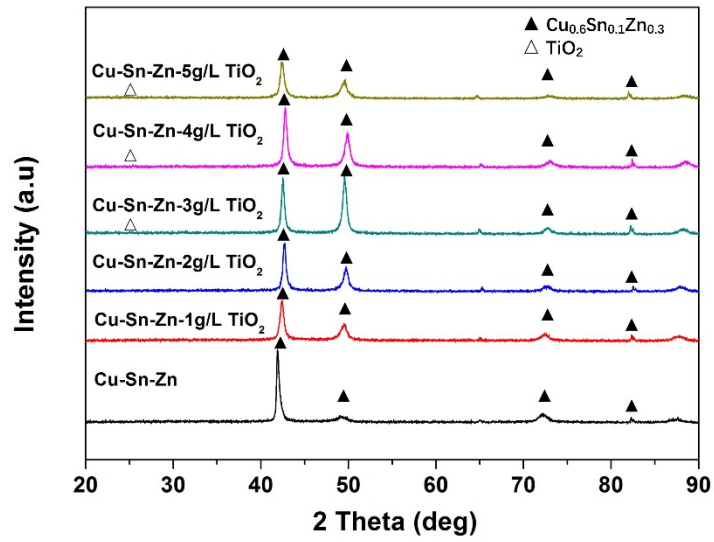


Fig. 1 XRD patterns of Cu-Sn-Zn and Cu-Sn-Zn-TiO<sub>2</sub> nano-composite coatings

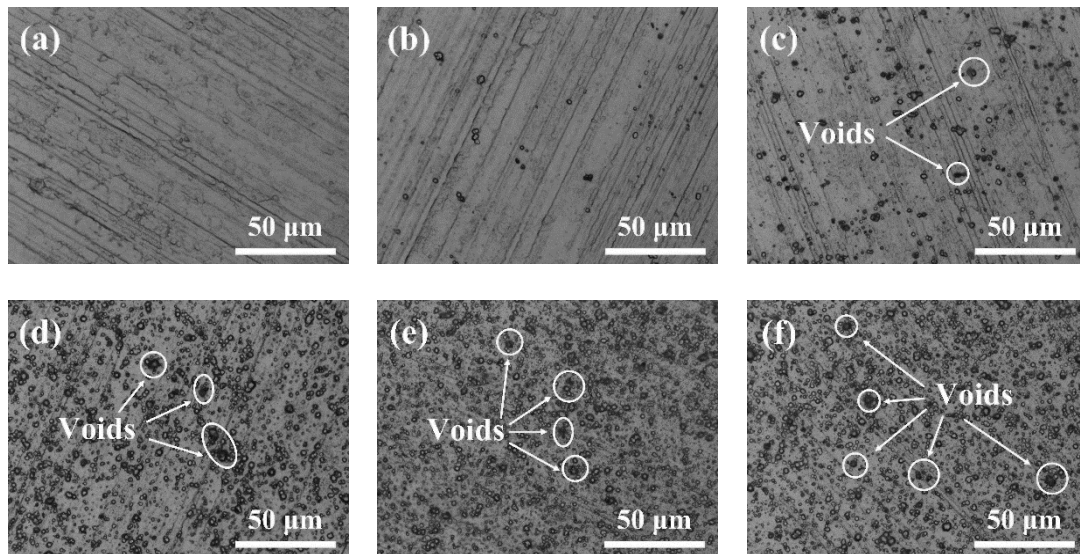


Fig. 2 Surface morphologies of six coating investigated in the current study: (a) Cu-Sn-Zn, (b) Cu-Sn-Zn-1g/L TiO<sub>2</sub>, (c) Cu-Sn-Zn-2g/L TiO<sub>2</sub>, (d) Cu-Sn-Zn-3g/L TiO<sub>2</sub>, (e) Cu-Sn-Zn-4g/L TiO<sub>2</sub>, and (f) Cu-Sn-Zn-5g/L TiO<sub>2</sub>.

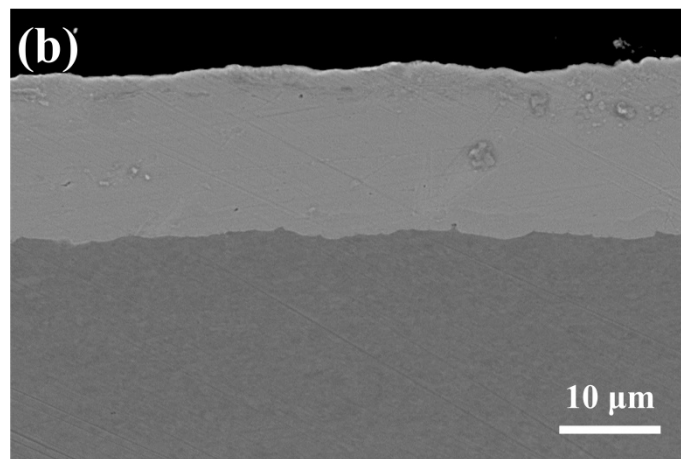
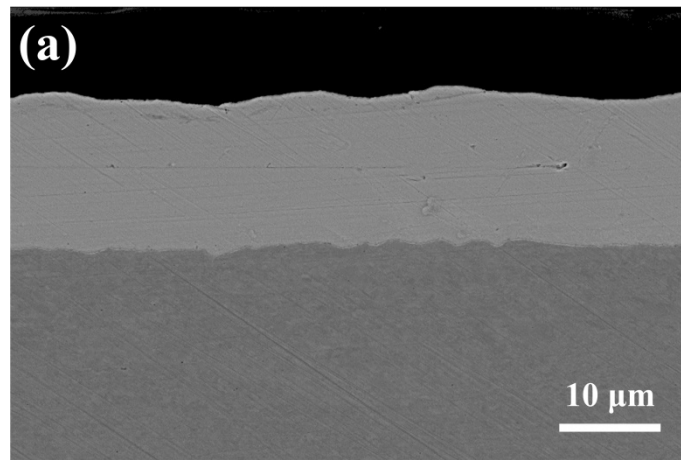


Fig. 3 Cross-section images of (a) Cu-Sn-Zn and (b) Cu-Sn-Zn-1g/L TiO<sub>2</sub> coatings

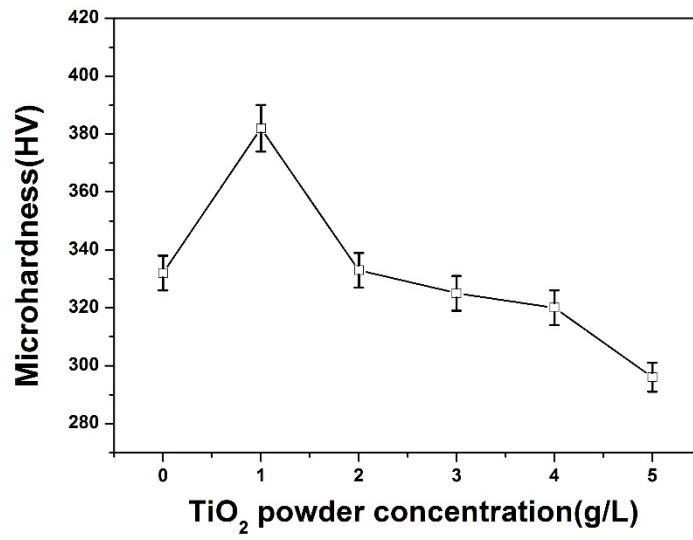


Fig. 4 Effect of TiO<sub>2</sub> concentration on microhardness of Cu-Sn-Zn-TiO<sub>2</sub> nano-composite coating.

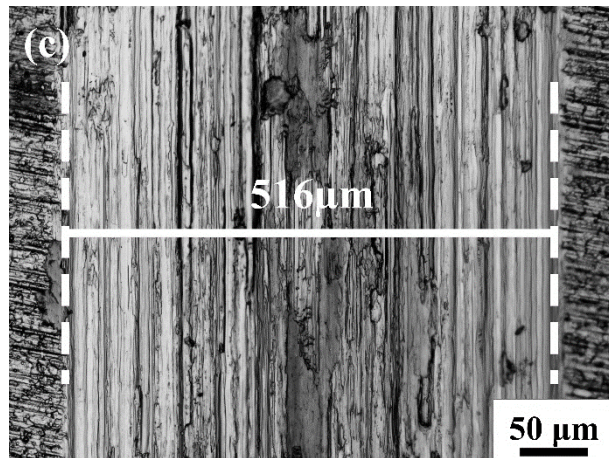
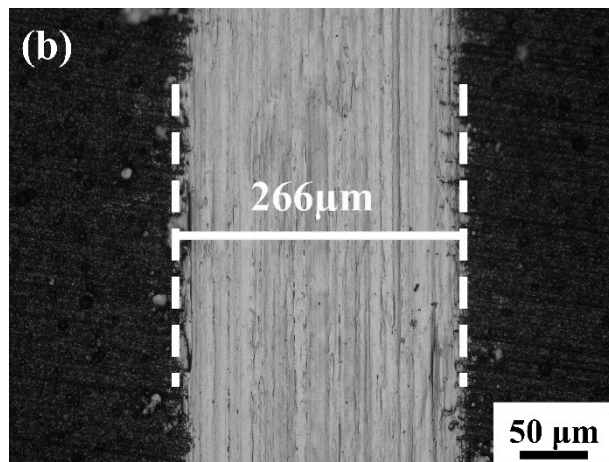
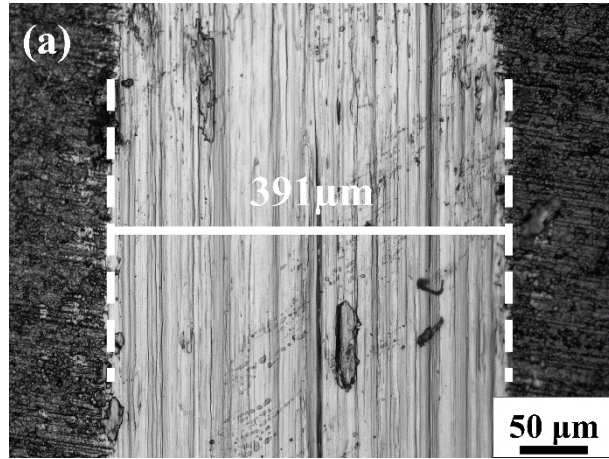


Fig. 5 Wear track images of (a) Cu-Sn-Zn, (b) Cu-Sn-Zn-1 g/L TiO<sub>2</sub> and (c) Cu-Sn-Zn-5 g/L TiO<sub>2</sub> coatings.

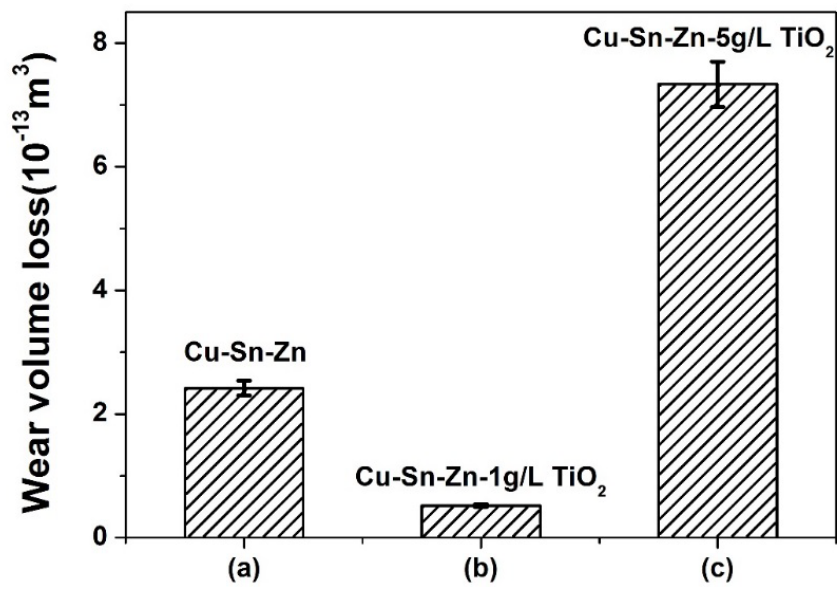


Fig. 6 Wear volume loss of (a) Cu-Sn-Zn, (b) Cu-Sn-Zn-1 g/L TiO<sub>2</sub> and (c) Cu-Sn-Zn -5 g/L TiO<sub>2</sub> coatings.

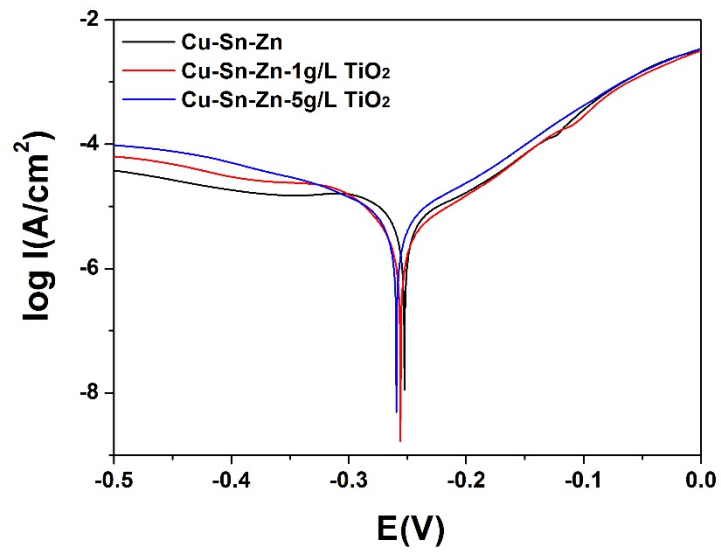


Fig. 7 Potentiodynamic polarization curves of (a) Cu-Sn-Zn, (b) Cu-Sn-Zn-1 g/L TiO<sub>2</sub> and (c) Cu-Sn-Zn -5 g/L TiO<sub>2</sub> coatings.

## Reference

- [1] A. Brenner, *Electrodeposition of alloys: principles and practice*, Elsevier 2013.
- [2] F. Walsh, C. Low, A review of developments in the electrodeposition of tin-copper alloys, *Surf. Coat. Technol.* 304 (2016) 246-262.
- [3] S. Yang, C. Ho, C. Chang, C. Kao, Strong Zn concentration effect on the soldering reactions between Sn-based solders and Cu, *J. Mater. Res.* 21 (2006) 2436-2439.
- [4] J.-W. Yoon, S.-B. Jung, Interfacial reactions and shear strength on Cu and electrolytic Au/Ni metallization with Sn-Zn solder, *J. Mater. Res.* 21 (2006) 1590-1599.
- [5] J.-E. Lee, K.-S. Kim, K. Suganuma, J. Takenaka, K. Hagio, Interfacial properties of Zn-Sn alloys as high temperature lead-free solder on Cu substrate, *Mater. Trans. JIM* 46 (2005) 2413-2418.
- [6] M. Date, K. Tu, T. Shoji, M. Fujiyoshi, K. Sato, Interfacial reactions and impact reliability of Sn-Zn solder joints on Cu or electroless Au/Ni (P) bond-pads, *J. Mater. Res.* 19 (2004) 2887-2896.
- [7] D. Yu, H. Xie, L. Wang, Investigation of interfacial microstructure and wetting property of newly developed Sn-Zn-Cu solders with Cu substrate, *J. Alloys Compd.* 385 (2004) 119-125.
- [8] C.-A. Hsu, M.-Y. Tu, Y.-F. Hsu, W.-H. Wang, The Precipitation Behavior of  $\alpha$ 1-Plate and  $\gamma$  Phase in Cu-Zn-Sn Shape Memory Alloys, *Mater. Trans. JIM* 47 (2006) 2427-2433.
- [9] M.C. Riglos, J. Pelegrina, M. Ahlers, Phase stability in Cu-Zn-based ternary alloys with elements of column 14, *Mater. Sci. Eng. A* 481 (2008) 504-508.
- [10] K. Neishi, T. Uchida, A. Yamauchi, K. Nakamura, Z. Horita, T. Langdon, Low-temperature superplasticity in a Cu-Zn-Sn alloy processed by severe plastic deformation, *Mater. Sci. Eng. A* 307 (2001) 23-28.
- [11] Y. Min, L. Xiuzhong, L. Xinghong, D. Jiahui, Development of Sn-Zn-Cu lead free solder, *Electronic Packaging Technology & High Density Packaging (ICEPT-HDP)*, 2010 11th International Conference on, IEEE, 2010, pp. 784-788.
- [12] C.-Y. Yu, J.-G. Duh, Stabilization of hexagonal Cu<sub>6</sub>(Sn, Zn)<sub>5</sub> by minor Zn doping of Sn-based solder joints, *Scr. Mater.* 65 (2011) 783-786.
- [13] L. Picincu, D. Pletcher, A. Smith, Electrochemistry of the SUCOPLATE® Electroplating Bath for the Deposition of a Cu-Zn-Sn Alloy; Part I: Commercial bath, *J. Appl. Electrochem.* 31 (2001) 387-394.
- [14] L. Picincu, D. Pletcher, A. Smith, Electrochemistry of the SUCOPLATE® Electroplating Bath for the Deposition of Cu-Zn-Sn Alloy; Part II: Influence of the concentration of bath components, *J. Appl. Electrochem.* 31 (2001) 395-402.

- [15] W. Miu, J. Ross, F. Lau, B. Fong, Studies on the electrodeposition of ternary copper-zinc-tin alloys, *Transactions of the IMF* 75 (1997) 137-139.
- [16] L. Wang, S. Kitamura, K. Obata, S. Tanase, T. Sakai, Multilayered Sn–Zn–Cu alloy thin-film as negative electrodes for advanced lithium-ion batteries, *J. Power Sources* 141 (2005) 286-292.
- [17] X.-K. He, B.-Z. Chen, G.-S. Hu, L.-F. Deng, N.-B. Zhou, W.-Z. Tian, Process of electroless plating Cu-Sn-Zn ternary alloy, *Trans. Nonferrous Met. Soc. China* 16 (2006) 223-228.
- [18] R. Rosley, S.S. Jikan, N.A. Badarulzaman, Production of Cu-Sn-Zn Ternary Alloy Coating via Electroplating, *Materials Science Forum*, *Trans Tech Publ*, 2017, pp. 400-403.
- [19] H. Capel, P. Shipway, S. Harris, Sliding wear behaviour of electrodeposited cobalt–tungsten and cobalt–tungsten–iron alloys, *Wear* 255 (2003) 917-923.
- [20] X. Shu, Y. Wang, C. Liu, W. Gao, Microstructure and properties of Ni–B–TiO<sub>2</sub> nano-composite coatings fabricated by electroless plating, *Materials Technology* 30 (2015) A41-A45.
- [21] Y. Wang, X. Shu, S. Wei, C. Liu, W. Gao, R. Shakoor, R. Kahraman, Duplex Ni–P–ZrO<sub>2</sub>/Ni–P electroless coating on stainless steel, *J. Alloys Compd.* 630 (2015) 189-194.
- [22] Y. Wang, Y. Ju, S. Wei, W. Gao, W. Lu, B. Yan, Au-Ni-TiO<sub>2</sub> Nano-Composite Coatings Prepared by Sol-Enhanced Method, *Journal of The Electrochemical Society* 161 (2014) D775-D781.
- [23] Y. Wang, G. Cheng, S.L. Tay, Y. Guo, X. Sun, W. Gao, Effects of Bi Addition on the Microstructure and Mechanical Properties of Nanocrystalline Ag Coatings, *Materials* 10 (2017) 932.
- [24] G. Cheng, F. Zhang, A. Ruimi, D.P. Field, X. Sun, Quantifying the effects of tempering on individual phase properties of DP980 steel with nanoindentation, *Mater. Sci. Eng. A* 667 (2016) 240-249.
- [25] G. Cheng, K.S. Choi, X. Hu, X. Sun, Application of Nano-Indentation Test in Estimating Constituent Phase Properties for Microstructure-Based Modeling of Multiphase Steels, *SAE Int. J. Engines* 10(2) (2017) 405-412.
- [26] G. Cheng, K.S. Choi, X. Hu, X. Sun, Determining individual phase properties in a multi-phase Q&P steel using multi-scale indentation tests, *Mater. Sci. Eng. A* 652 (2016) 384-395.
- [27] G. Cheng, E.I. Barker, E.V. Stephens, K.S. Choi, X. Sun, Quantifying Grain Level Stress-Strain Behavior for AM40 via Instrumented Microindentation, *MRS Advances* 1 (2016) 761-772.
- [28] M. Hiratani, H.M. Zbib, M.A. Khaleel, Modeling of thermally activated

dislocation glide and plastic flow through local obstacles, *Int. J. Plast.* 19 (2003) 1271-1296.

[29] M. Rhee, J. Hirth, H. Zbib, A superdislocation model for the strengthening of metal matrix composites and the initiation and propagation of shear bands, *Acta Mater.* 42 (1994) 2645-2655.

[30] L. Chen, L. Wang, Z. Zeng, T. Xu, Influence of pulse frequency on the microstructure and wear resistance of electrodeposited Ni–Al<sub>2</sub>O<sub>3</sub> composite coatings, *Surf. Coat. Technol.* 201 (2006) 599-605.

[31] M. Palaniappa, S. Seshadri, Friction and wear behavior of electroless Ni–P and Ni–W–P alloy coatings, *Wear* 265 (2008) 735-740.

[32] Y. Wang, H. Wang, Wear resistance of laser clad Ti<sub>2</sub>Ni<sub>3</sub>Si reinforced intermetallic composite coatings on titanium alloy, *Appl. Surf. Sci.* 229 (2004) 81-86.

[33] M. Srivastava, V.K. William Grips, A. Jain, K.S. Rajam, Influence of SiC particle size on the structure and tribological properties of Ni–Co composites, *Surf. Coat. Technol.* 202 (2007) 310-318.

[34] J. Archard, Contact and rubbing of flat surfaces, *J. Appl. Phys.* 24 (1953) 981-988.

[35] J. Archard, W. Hirst, The wear of metals under unlubricated conditions, *Proceedings of the Royal Society of London A: Mathematical, Physical and Engineering Sciences*, The Royal Society, 1956, pp. 397-410.

[36] Y. Wang, S.L. Tay, S. Wei, C. Xiong, W. Gao, R.A. Shakoor, R. Kahraman, Microstructure and properties of sol-enhanced Ni-Co-TiO<sub>2</sub> nano-composite coatings on mild steel, *J. Alloys Compd.* 649 (2015) 222-228.

[37] G. Cheng, S. Sriram, M. Bhaskaran, T.A. Venkatesh, Nanoindentation response of piezoelectric nano-islands, *Appl. Phys. Lett.* 105 (2014) 122902.

[38] R. Saha, W.D. Nix, Effects of the substrate on the determination of thin film mechanical properties by nanoindentation, *Acta Mater.* 50 (2002) 23-38.

[39] N. Nakamura, H. Ogi, M. Hirao, Elastic constants of chemical-vapor-deposition diamond thin films: resonance ultrasound spectroscopy with laser-Doppler interferometry, *Acta Mater.* 52 (2004) 765-771.

[40] D. Li, S. Zhang, W. Yang, W. Zhang, Corrosion Monitoring and Evaluation of Reinforced Concrete Structures Utilizing the Ultrasonic Guided Wave Technique, *International Journal of Distributed Sensor Networks* 10 (2014) 827130.

[41] W. Shen, D. Li, S. Zhang, J. Ou, Analysis of wave motion in one-dimensional structures through fast-Fourier-transform-based wavelet finite element method, *Journal of Sound and Vibration* 400 (2017) 369-386.